Coordinate Interleaved Orthogonal Design With Media-Based Modulation

Ibrahim Yildirim, *Graduate Student Member, IEEE*,
Ertugrul Basar, *Senior Member, IEEE*,
and Ibrahim Altunbas, *Senior Member, IEEE*

***Abstract*—In this work, we propose a new multiple-input multiple-output (MIMO) concept, which is called coordinate interleaved orthogonal design with media-based modulation (CIOD-MBM). The proposed two novel CIOD-MBM schemes provide improved data rates as well as diversity gain while enabling hardware simplicity using a single radio frequency (RF) chain. Moreover, using the equivalent channel model, a reduced complexity can be obtained for maximum likelihood (ML) detection of the proposed system. Using computer simulations, it is shown that CIOD-MBM schemes provide remarkably better performance against the conventional MBM and CIOD systems.**

***Index Terms*—Coordinate interleaved orthogonal design, index modulation, media-based modulation, space-time coding.**

I. Introduction

Index modulation (IM) schemes, which achieve high data rates while reducing hardware costs in the transmitter, have recently received remarkable attention [1]. Spatial modulation (SM), the well-known member of the IM family, conveys information by transmit antenna indices as well as conventional phase shift keying (PSK) or quadrature amplitude modulation (QAM) methods [2]. The media-based modulation (MBM) scheme, which is proposed as an avant-garde digital transmission method for rich scattering environments, is considered as an alternative to SM [3]. In MBM systems, the current distributions of the reconfigurable antennas are changed by means of various elements, such as PIN diodes, varactors, micro-electro-mechanical switches, and so on, hence, different channel fading realizations, which is called as channel states, are obtained. Using the on/off status of the parasitic elements called radio frequency (RF) mirrors, different radiation patterns are acquired. Unlike SM, since the spectral efficiency in the MBM varies linearly proportional to the number of RF mirrors, it is sufficient to increase the number of RF mirrors in a bid to achieve high data rates.

Existing multiple-input multiple-output (MIMO) techniques such as SM, quadrature SM (QSM) and generalized SM (GSM) can be integrated with MBM to achieve promising results. In [4], GSM is adopted to MBM in order to enhance spectral efficiency and error performance. Combining QSM and MBM innovatively, promising results are obtained by quadrature channel modulation (QCM) [5]. Space-time coding concept also can be merged with MBM to increase the diversity gain. To this end, space-time channel modulation (STCM) method is proposed in [6], which combines Alamouti's famous space-time block code (STBC) with MBM. Additionally, considering the flexibility of IM techniques, time-indexed based SM and MBM schemes are proposed in [7]. In recent past, since MBM systems are prone to increase physical layer security, various secret transmission scenarios are proposed to enable high secrecy capacity using appropriate designs [8]. Differential MBM (DMBM) [9] provides a linear programming-based decoding concept, which has alleviated the requirement of channel sounding when it is hard to get accurate channel state information (CSI) at the destination. Furthermore, effective compress sensing [10] and message passing [11] based decoding methods for MBM and IM systems are proposed using advanced signal processing techniques. In [12], a comprehensive frame for space-time coded MBM systems is presented and miscellaneous diversity gains are obtained in the proposed system. In order to overcome fractional bit problems in IM systems, authors propose fractional MBM with golden angle modulation (GAM-MBM) in [13] by making use of the symmetrical structure of GAM.

In this paper, we introduce coordinate interleaved orthogonal design MBM (CIOD-MBM) concept, which provides diversity gain as well as increased spectral efficiency while assuring hardware simplicity using a single RF chain. The focus of this work is to bring the desirable benefits of CIOD, such as enabling low complexity maximum likelihood (ML) detection opportunity and simple transmitter structure, into the area of interest of MBM. In this context, two promising CIOD-MBM schemes, which use a single active antenna during the transmission, are presented. Furthermore, the theoretical average bit error probability (ABEP) of the proposed CIOD-MBM schemes are derived. Afterwards, the supremacy of the proposed CIOD-MBM concept is demonstrated via computer simulations in terms of error performance and obtained numerical results are verified with theoretical results.

II. Coordinate Interleave Orthogonal Designs for Media-Based Modulation

In this section, we introduce the system model and the working principle of CIOD-MBM schemes under quasi-static flat Rayleigh fading channel. $N_r \times N_t$ MIMO transmission scenario is considered by assuming each transmit antenna has N_{rf} RF mirrors. Here, while the selected active antennas are set to a single channel state only at a time slot, signal reception is done by all receive antennas.

The essential principle of CIOD is to achieve diversity gain by transmitting symbols through different channels in two different time slots. Due to the transmission using a single active antenna, reduced hardware cost is obtained keeping only one RF chain. Unlike traditional STBCs, signal constellation must be rotated at a specific angle to ensure the full diversity of CIODs [14]. The CIOD signal matrix for the system with two transmit antennas is as follows

$$\begin{bmatrix} \tilde{s_0} & 0 \\ 0 & \tilde{s_1} \end{bmatrix} \tag{1}$$

where $\tilde{s_0} = x_0^{\Re} + jx_1^{\Im}$ and $\tilde{s_1} = x_1^{\Re} + jx_0^{\Im}$ are transmitted symbols, which are obtained by partitioning x_i ($i \in \{0, 1\}$) symbol into its real ($x_i^{\Re}$) and imaginary ($x_i^{\Im}$) part. Here, the columns and rows of the CIOD signal matrix represent time slots and transmit antennas, respectively, and x_0 and x_1 are selected from a signal constellation formed by rotating the ordinary M-ary signal constellation with a certain angle. Moreover, M is the modulation order of PSK/QAM constellation. For instance, the optimum rotation angle in the quadrature PSK (QPSK) constellation is 13.2885° for the conventional CIOD in (1) [14].

Manuscript received December 24, 2020; accepted February 7, 2021. Date of publication February 15, 2021; date of current version April 2, 2021. This work was supported by the Scientific and Technological Research Council of Turkey (TUBITAK) under Grant 117E869. The review of this article was coordinated by Prof. Yong Liang Guan. *(Corresponding author: Ibrahim Yildirim.)*

Ibrahim Yildirim and Ibrahim Altunbas are with the Electronics and Communications Enginnering, Istanbul Technical University, Istanbul, Sariyer 34469, Turkey (e-mail: yildirimib@itu.edu.tr; ibraltunbas@itu.edu.tr).

Ertugrul Basar is with the Koç University, Istanbul 34450, Turkey (e-mail: ebasar@ku.edu.tr).

Digital Object Identifier 10.1109/TVT.2021.3059325

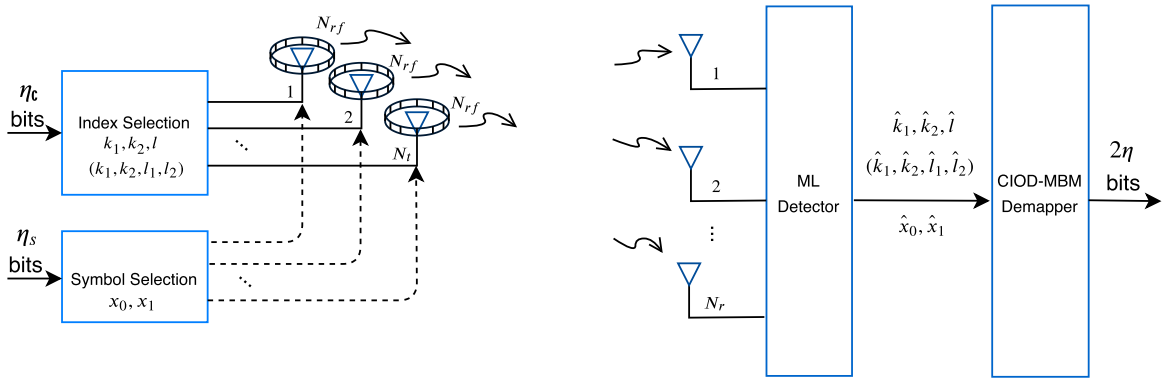

Fig. 1. Block diagram of $N_r \times N_t$ MIMO system which is employed by CIOD-MBM schemes.

Considering peculiarities of CIOD, two novel CIOD-MBM schemes are designed for a given MIMO system. The generalized baseband received signal model of the CIOD-MBM schemes can be expressed as

$$\mathbf{Y} = \mathbf{HX} + \mathbf{N} \tag{2}$$

where $\mathbf{Y} \in \mathbb{C}^{N_r \times 2}$ is matrix of the received signals in two different time slots, $\mathbf{H} \in \mathbb{C}^{N_r \times N_t 2^{N_{rf}}}$ is the channel matrix, and $\mathbf{N} \in \mathbb{C}^{N_r \times 2}$ is the noise sample matrix, respectively. At the same time, $\mathbf{X} \in \mathbb{C}^{N_t 2^{N_{rf}} \times 2}$ represents the CIOD matrix, which is designed for two different MBM schemes. The elements of $\mathbf{H}$ and $\mathbf{N}$ follow zero mean independent and identically complex Gaussian distribution with variances 1 and N_0, respectively.

A. CIOD-MBM I Scheme

The block diagram of CIOD-MBM I scheme is given in Fig. 1, where $\eta_c = \log_2(N_t/2) + N_{rf}$ and $\eta_s = 2\log_2(M)$ respectively denote the number of index and symbol bits sent in two slots. The spectral efficieny of CIOD-MBM I scheme is calculated as

$$\eta = \left(\log_2(N_t/2) + N_{rf} + 2\log_2(M)\right)/2 \quad \text{bit/s/Hz.} \tag{3}$$

Before determining the active channel state, available antennas are divided into two groups. Then, using the first $\log_2(N_t/2)$ bits, active antenna index k_1 is determined for the first time slot. The group, to which the first active antenna belongs, is omitted in the second selection. For the determined antenna, active channel state l is chosen depending on N_{rf} bits. In the second time slot, second active antenna index k_2 is determined as $k_2 = N_t/2 + k_1$. Then, lth channel state is also selected in the second time slot as similar as first time slot. After all, transmitted symbols x_0 and x_1 are chosen by the aid of last $2\log_2(M)$ bits. By creating $(N_t/2)2^{N_{rf}}$ possible transmission vectors with $\log_2(N_t/2) + N_{rf}$ index bits, an additional dimension is obtained in order to convey information in addition to the conventional modulation methods. Here, each index bit group has different k_1, k_2 and l indices combination. Following these procedures, the transmission matrix $\mathbf{X}$ is constructed as

$$\mathbf{X} = \left[\begin{array}{c|c|c|c} 0\ldots & \overbrace{\begin{matrix}\ldots & \tilde{s}_0 & \ldots \\ \ldots & 0 & \ldots\end{matrix}}^{l\text{th state}} & \ldots & \begin{matrix}\ldots & 0 & \ldots \\ \ldots & \tilde{s}_0 & \ldots\end{matrix} \\ 0\ldots & \underbrace{\qquad\qquad}_{k_1\text{th antenna}} & \ldots & \underbrace{\qquad\qquad}_{k_2\text{the antenna}} \end{array}\right]^2 \tag{4}$$

where $(.)^T$ denotes matrix transpose, and possible channel realizations and time slots are represented by rows and columns, respectively. In (4), dots represent the zeros, and $\tilde{s}_0$ and $\tilde{s}_1$ are the only non-zero entries of $\mathbf{X}$. The rows of $\mathbf{X}$ are divided into N_t different group, each of which has $2^{N_{rf}}$ dimension, by vertical lines.

TABLE I
CIOD-MBM INDEX MAPPING RULE FOR $N_t = 4$ AND $N_{rf} = 1$

Bits	$\{k_1, k_2\}$	l	$\mathbf{X}^T$
00	$\{1,3\}$	1	$\left[\begin{array}{cc\|cc\|cc\|cc} \tilde{s_0} & 0 & 0 & 0 & 0 & 0 & 0 & 0 \\ 0 & 0 & 0 & 0 & \tilde{s_1} & 0 & 0 & 0 \end{array}\right]$
01	$\{1,3\}$	2	$\left[\begin{array}{cc\|cc\|cc\|cc} 0 & \tilde{s_0} & 0 & 0 & 0 & 0 & 0 & 0 \\ 0 & 0 & 0 & 0 & 0 & \tilde{s_1} & 0 & 0 \end{array}\right]$
10	$\{2,4\}$	1	$\left[\begin{array}{cc\|cc\|cc\|cc} 0 & 0 & \tilde{s_0} & 0 & 0 & 0 & 0 & 0 \\ 0 & 0 & 0 & 0 & 0 & 0 & \tilde{s_1} & 0 \end{array}\right]$
11	$\{2,4\}$	2	$\left[\begin{array}{cc\|cc\|cc\|cc} 0 & 0 & 0 & \tilde{s_0} & 0 & 0 & 0 & 0 \\ 0 & 0 & 0 & 0 & 0 & 0 & 0 & \tilde{s_1} \end{array}\right]$

The CIOD-MBM I scheme provides full diversity when the minimum determinant of the distance matrix is maximized. If $\mathbf{X}$ is transmitted and erroneously detected as $\hat{\mathbf{X}}$, under full rank condition, the minimum coding gain distance is given by

$$\delta_{\min} = \min_{\mathbf{X}, \hat{\mathbf{X}}, \mathbf{X} \neq \hat{\mathbf{X}}} \det[(\mathbf{X} - \hat{\mathbf{X}})(\mathbf{X} - \hat{\mathbf{X}})^H]. \tag{5}$$

In CIOD-MBM I, the rotation angle, which guarantees full diversity, is calculated as 13.2885° for QPSK. If the system with $N_t = 4$, $N_{rf} = 1$ and $M = 4$ (QPSK) is considered to exemplify the working mechanism of CIOD-MBM I, spectral efficiency (η) is calculated as 3 b/s/Hz. In two time slots, $2\eta = 6$ incoming bits are processed as follows:

$$\mathbf{b} = [\ \underbrace{1\,0}_{\log_2(N_t/2)+N_{rf}}\ \underbrace{1\,1}_{\log_2(M)}\ \underbrace{1\,0}_{\log_2(M)}\ ]. \tag{6}$$

Using the mapping rule of the CIOD-MBM as shown in Table I, first $\log_2(N_t/2) + N_{rf} = 2$ bits assign the active antenna index set $\{k_1, k_2\}$ and channel state l, respectively. After the two active channel states are separately obtained, the next [1 1] bits modulate to determine rotated QPSK symbol $x_0 = 0.2299 - j0.9732$. Thereafter, last two bits [1 0] specify the $x_1 = -0.9732 - j0.2299$ from rotated QPSK symbol set. Finally, CIOD-MBM I matrix is obtained as

$$\mathbf{X} = \left[\begin{array}{cc|c|cc|c|cc} \underbrace{0\ 0}_{\text{ant. 1}} & & x_0^{\Re} + jx_1^{\Im} & 0 & \underbrace{0\ 0}_{\text{ant. 3}} & & 0 & 0 \\ \underbrace{0\ 0}_{\text{ant. 1}} & & \underbrace{0}_{\text{ant. 2}} & 0 & \underbrace{0\ 0}_{\text{ant. 3}} & & x_1^{\Re} + j\underbrace{x_0^{\Im}}_{\text{ant. 4}} & 0 \end{array}\right]^T. \tag{7}$$

B. Ciod-Mbm Ii

The main motivation of this system is to increase the spectral efficiency of the CIOD-MBM I scheme while maintaining diversity

gain and other inherent advantages. The block diagram of CIOD-MBM II can be seen from Fig. 1, which the terms in parentheses represent active antenna and channel state indices of CIOD-MBM II, for $\eta_c = N_{rf} - 1 + 2\log_2(N_t)$ and $\eta_s = 2\log_2(M)$. In the CIOD-MBM II scheme, which is inspired by QSM and QCM [5], active transmit antennas are individually selected for real and imaginary parts of $\tilde{s_0}$ and $\tilde{s_1}$ symbols. The spectral efficiency of the CIOD-MBM II is calculated as

$$\eta = \left(N_{rf} - 1 + 2\log_2(N_t) + 2\log_2(M)\right)/2 \quad \text{bit/s/Hz}. \tag{8}$$

In order to guarantee the utilization of a single RF chain at a single time slot, a total of $2^{N_{rf}}$ channel states are divided into two groups similar to the CIOD-MBM I. In this method, l_1 and l_2 represent the active channel states for all antennas in the first and second time slots, respectively. By selecting only one channel state for each antenna in a time slot, it is prevented to set an antenna to more than one channel state at the same time. The first $2N_{rf} - 1$ bits decide the active channel state l_1 for the initial time slot. After determining the group, to which l_1 belongs, active second channel state l_2 is determined as $l_2 = 2^{N_{rf}}/2 + l_1$. Using $2\log_2(N_t)$ bits, active antennas k_1 and k_2 are selected for real and imaginary parts of transmitted symbols, respectively. Then, the last $2\log_2(M)$ bits are used to specify the modulated symbols x_0 and x_1 from rotated M-ary constellations. Here, an additional dimension and increased bit rate are obtained similar to the CIOD-MBM I scheme due to η_c bits. The generalized transmission matrix is given as, equation (9), shown at the bottom of this page, where possible channel realizations and time slots are represented by rows and columns, respectively. Here, all entries of the $\mathbf{X}$, except $x_0^{\Re}$, $jx_1^{\Im}$, $x_1^{\Re}$, and $jx_0^{\Im}$, are equal to 0 and dots represent the zero entries. In this representation, all antennas are grouped according to their channel states and separated by vertical lines. For selected channel states, N_t antennas are available in both time slots.

The system with $N_t = 2$, $N_{rf} = 2$ and $M = 4$ is explained by the following example. In this scenario, the spectral efficiency is calculated as $\eta = 3.5$ bit/s/Hz. 30° is the optimum angle that ensures full diversity and maximizes the $\delta_{\min}$ for QPSK in CIOD-MBM II while 8.6° is the optimum angle for 16-QAM. For two time slots, it is assumed that incoming bits are arranged as follows:

$$\mathbf{b} = [\underbrace{1\,0\,1}_{N_{rf}-1+2\log_2(N_t)}\ \underbrace{0\,1}_{\log_2(M)}\ \underbrace{1\,1}_{\log_2(M)}]. \tag{10}$$

With the aid of Table II, active antenna set $\{k_1, k_2\}$ and channel index set $\{l_1, l_2\}$ are determined by the first $\eta_c = 3$ index bits. As seen from Table II, the state $l_1 = 2$ is active of the antenna $k_1 = 1$ and $k_2 = 2$ for the transmission of $x_0^{\Re}$ and $jx_1^{\Im}$ in first time slot, respectively, while the state $l_2 = 4$ is active of the antenna $k_1 = 1$ and $k_2 = 2$, respectively, for the transmission of $x_1^{\Re}$ and $jx_0^{\Im}$ in second time slot. Then, using η_s symbol bits, x_0 and x_1 are chosen from the rotated constellation as $-0.5 + j0.866$ and $0.5 - j0.866$, respectively. In the final stage, transmission matrix is constructed as

$$\mathbf{X} = \left[\begin{array}{c|c|c|c} \underbrace{\begin{matrix}0&0\\0&0\end{matrix}}_{\text{state 1}} & \begin{matrix}-0.5-j0.866 & 0\\ \underbrace{0}_{\text{state 2}} & 0\end{matrix} & \underbrace{\begin{matrix}0&0\\0&0\end{matrix}}_{\text{state 3}} & \begin{matrix}0 & 0 & 0.5 & \underbrace{j0.866}_{\text{state 4}}\end{matrix} \end{array}\right]^T. \tag{11}$$

TABLE II
CIOD-MBM II INDEX MAPPING RULE FOR $N_t = 2$ AND $N_{rf} = 2$

Bits	$\{l_1, l_2\}$-$\{k_1, k_2\}$	$\mathbf{X}^T$
000	{1,3} - {1,1}	$\left[\begin{array}{cc\|cc\|cc\|cc} x_0^{\Re}+jx_1^{\Im} & 0 & 0 & 0 & 0 & 0 & 0 & 0 \\ 0 & 0 & 0 & 0 & x_1^{\Re}+jx_0^{\Im} & 0 & 0 & 0 \end{array}\right]$
001	{1,3} - {1,2}	$\left[\begin{array}{cc\|cc\|cc\|cc} x_0^{\Re}+jx_1^{\Im} & 0 & 0 & 0 & 0 & 0 & 0 & 0 \\ 0 & 0 & 0 & 0 & x_1^{\Re} & jx_0^{\Im} & 0 & 0 \end{array}\right]$
010	{1,3} - {2,1}	$\left[\begin{array}{cc\|cc\|cc\|cc} x_0^{\Re} & jx_1^{\Im} & 0 & 0 & 0 & 0 & 0 & 0 \\ 0 & 0 & 0 & 0 & x_1^{\Re}+jx_0^{\Im} & 0 & 0 & 0 \end{array}\right]$
011	{1,3} - {2,2}	$\left[\begin{array}{cc\|cc\|cc\|cc} x_0^{\Re} & jx_1^{\Im} & 0 & 0 & 0 & 0 & 0 & 0 \\ 0 & 0 & 0 & 0 & x_1^{\Re} & jx_0^{\Im} & 0 & 0 \end{array}\right]$
100	{2,4} - {1,1}	$\left[\begin{array}{cc\|cc\|cc\|cc} 0 & 0 & x_0^{\Re}+jx_1^{\Im} & 0 & 0 & 0 & 0 & 0 \\ 0 & 0 & 0 & 0 & 0 & 0 & x_1^{\Re}+jx_0^{\Im} & 0 \end{array}\right]$
101	{2,4} - {1,2}	$\left[\begin{array}{cc\|cc\|cc\|cc} 0 & 0 & x_0^{\Re}+jx_1^{\Im} & 0 & 0 & 0 & 0 & 0 \\ 0 & 0 & 0 & 0 & 0 & 0 & x_1^{\Re} & jx_0^{\Im} \end{array}\right]$
110	{2,4} - {2,1}	$\left[\begin{array}{cc\|cc\|cc\|cc} 0 & 0 & x_0^{\Re} & jx_1^{\Im} & 0 & 0 & 0 & 0 \\ 0 & 0 & 0 & 0 & 0 & 0 & x_1^{\Re}+jx_0^{\Im} & 0 \end{array}\right]$
111	{2,4} - {2,2}	$\left[\begin{array}{cc\|cc\|cc\|cc} 0 & 0 & x_0^{\Re} & jx_1^{\Im} & 0 & 0 & 0 & 0 \\ 0 & 0 & 0 & 0 & 0 & 0 & x_1^{\Re} & jx_0^{\Im} \end{array}\right]$

C. ML Detection for Proposed CIOD-MBM Schemes

As mentioned previous sections, one of the major advantages of CIOD is its symbol-by-symbol decoding possibility while keeping ML complexity remarkably reduced. In this sense, in the proposed CIOD-MBM I scheme, the equivalent system model of (2) is obtained by

$$\mathbf{y}_{eq} = \mathbf{H}_{eq}\mathbf{x}_{eq} + \mathbf{n}_{eq} \tag{12}$$

where $\mathbf{y}_{eq} \in \mathbb{C}^{4N_r \times 1}$, $\mathbf{x}_{eq} = [x_0^{\Re}\ x_0^{\Im}\ x_1^{\Re}\ x_1^{\Im}]^T$ and $\mathbf{n}_{eq} \in \mathbb{C}^{4N_r \times 1}$ represent the equivalent received signal vector, the equivalent transmitted symbols and the equivalent noise vector, respectively. The construction of generalized $\mathbf{y}_{eq}$ is shown by

$$\mathbf{y}_{eq} = [y_{1,1}^{\Re}\ y_{2,1}^{\Re} \dots y_{N_r,1}^{\Re}\ y_{1,1}^{\Im} \dots y_{N_r,1}^{\Im} \dots y_{1,2}^{\Re} \dots y_{N_r,2}^{\Im}]^T \tag{13}$$

where $y_{r,t}$ stands for received signal at rth receive antenna in tth time slot.

Furthermore, $\mathbf{H}_{eq} \in \mathbb{C}^{4N_r \times 4}$ denotes the equivalent channel matrix, which is specified in (14), shown at the bottom of the next page, for CIOD-MBM I. In this notation, h_{r,m_i} ($i \in \{1, 2\}$) represents channel fading coefficients between the selected active channel state (m_i) and rth receive antennas, where m_i is chosen from the possible $N_t 2^{N_{rf}}$ channel realizations depending on k and l sets. Because of the orthogonality of columns, the equivalent channel matrix is decomposed as $\mathbf{H}_{eq} = [\mathcal{H}_1\ \mathcal{H}_2]$ where $\mathcal{H}_1 \in \mathbb{C}^{4N_r \times 2}$ and $\mathcal{H}_2 \in \mathbb{C}^{4N_r \times 2}$ represent first two and last two columns of $\mathbf{H}_{eq}$. It can be easily observed that $\mathcal{H}_1$ and $\mathcal{H}_2$ are orthogonal each other, therefore, x_0 and x_1 are individually decoded for CIOD-MBM I.

As is common, considering the perfect CSI in CIOD-MBM I, ML detection is employed at the receiver by

$$[\hat{x_0}, \hat{x_1}, \hat{k}_1, \hat{k}_2, \hat{l}] = \arg \min_{x_0, x_1, k_1, k_2, l} \|\mathbf{y} - \mathbf{H}\mathbf{X}\|^2 \tag{15}$$

$$\mathbf{X} = \begin{bmatrix} 0 \dots & \dots\ \overbrace{x_0^{\Re}}\ k_1 \dots \overbrace{jx_1^{\Im}}\ k_2 \dots & \dots & \dots\ 0\ \dots & \dots 0 \\ 0 \dots & \underbrace{\dots\ 0\ \dots}_{l_1\text{thstate}} & \dots & \underbrace{\dots\ \overbrace{x_1^{\Re}}\ k_1 \dots \overbrace{jx_0^{\Im}}\ k_2 \dots}_{l_2\text{thstate}} & \dots 0 \end{bmatrix}^T \tag{9}$$

where $\|.\|$ represents the Euclidean norm. Similarly, the detection of the index bits is performed by minimization over k_1, k_2, l_1, l_2 indices in (15) instead of k_1, k_2, l in CIOD-MBM II scheme.

In CIOD-MBM I, considering all possible channel realizations, minimum ML decision metrics of x_0 and x_1 are separately obtained by

$$d_0^{(k_1,l)} = \min_{x_0} \left\| \mathbf{y} - \mathcal{H}_1 [x_0^{\Re}\ x_0^{\Im}]^T \right\|^2,$$
$$d_1^{(k_2,l)} = \min_{x_1} \left\| \mathbf{y} - \mathcal{H}_2 [x_1^{\Re}\ x_1^{\Im}]^T \right\|^2. \quad (16)$$

Thereafter, the minimum ML decision metric for a corresponding antenna and antenna state indices (k_1, k_2, l) is calculated by $d^{(k_1,k_2,l)} = d_0^{(k_1,l)} + d_1^{(k_2,l)}$. After obtaining all $d^{(k_1,k_2,l)}$, the most likely antenna and antenna state indices combination is determined by $(\hat{k}_1, \hat{k}_2, \hat{l}) = \arg\min_{(k_1,k_2,l)} d^{(k_1,k_2,l)}$. Using the most likely channel realizations, the transmitted data symbols are estimated by $(\hat{x}_0, \hat{x}_1) = (x_0^{(k_1,l)}, x_1^{(k_2,l)})$.

After the demapping process, decoded bits are obtained at the receiver. Thanks to the equivalent model, the number of calculated metrics is reduced from $2^{\eta_c} M^2$ to $2^{\eta_c} 2M$ for CIOD-MBM I scheme while conventional CIOD and CIOD-SM respectively consider $2^{\eta_c} 2M$ and $2^{\eta_c} M^2$ metrics. Due to the non-orthogonality of the equivalent channel matrix for CIOD-MBM II, brute-force ML detection is performed as in (15) with a complexity order of $2^{\eta_c} M^2$.

III. Performance Analysis

By the aid of union bounding technique, bit error performance of CIOD-MBM schemes are obtained [15]. Assuming that $\mathbf{X}$ is transmitted and incorrectly detected as $\hat{\mathbf{X}}$, the ABEP is approximately calculated by

$$P_b \approx \frac{1}{2\eta 2^{2\eta}} \sum_{\mathbf{X}} \sum_{\hat{\mathbf{X}}} P(\mathbf{X} \to \hat{\mathbf{X}})\, e(\mathbf{X}, \hat{\mathbf{X}}) \quad (17)$$

where pairwise bit error probability (PEP) and the number of bit errors are represented by $P(\mathbf{X} \to \hat{\mathbf{X}})$ and $e(\mathbf{X}, \hat{\mathbf{X}})$ respectively.

The conditional PEP (CPEP) for the CIOD-MBM schemes can be obtained as

$$P(\mathbf{X} \to \hat{\mathbf{X}} | \mathbf{H}) = Q\left(\sqrt{\Delta/(2N_0)}\right) \quad (18)$$

where $\Delta = \|\mathbf{H}(\mathbf{X} - \hat{\mathbf{X}})\|_{\mathrm{F}}^2$, $\|.\|_{\mathrm{F}}^2$ is the Frobenius norm and $Q(x)$ is the well-known Q-function, which is also represented as $Q(x) = 1/\pi \int_0^{\pi/2} e^{-x^2/\sin^2\theta} d\theta$. By means of this alternative version of the Q-function and the moment generating function of $\|\mathbf{H}(\mathbf{X} - \hat{\mathbf{X}})\|_{\mathrm{F}}^2$ [16], the unconditional PEP is given by

$$P(\mathbf{X} \to \hat{\mathbf{X}}) = \frac{1}{\pi} \int_0^{\frac{\pi}{2}} \left(\frac{\sin^2\theta}{\sin^2\theta + \frac{\lambda_1}{4N_0}} \right)^{N_r} \left(\frac{\sin^2\theta}{\sin^2\theta + \frac{\lambda_2}{4N_0}} \right)^{N_r} d\theta \quad (19)$$

where λ_d, $d \in \{1, 2\}$ stand for the eigenvalues of the $(\mathbf{X} - \hat{\mathbf{X}})(\mathbf{X} - \hat{\mathbf{X}})^H$ matrix, which is not equal to zero.

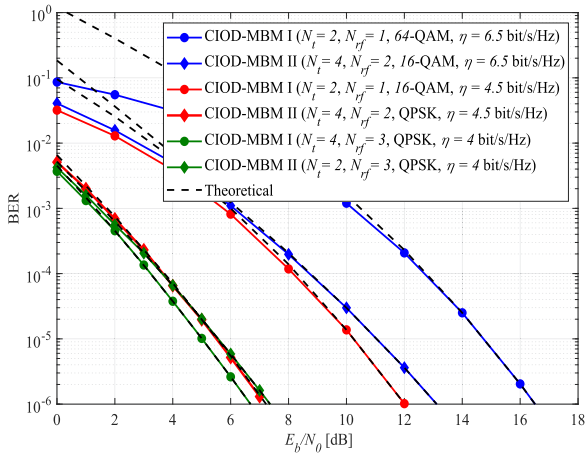

Fig. 2. Theoretical ABEP and computer simulated BER of the CIOD-MBM schemes under various N_t, N_{rf} and M values for $N_r = 4$.

IV. Simulation Results

In order to evaluate the error performance of the CIOD-MBM schemes, BER results are produced using computer simulations under varying system parameters. Considering conventional SIMO, MBM [3], CIOD [14] and CIOD-SM [17] as reference systems, BER results are obtained with respect to E_b/N_0, where E_b is the average transmitted energy per bit.

In Fig. 2, theoretical ABEP results of both CIOD-MBM schemes are obtained to compare the BER results obtained by computer simulations. As can be clearly seen, the theoretical curves are perfectly matched with the computer simulation results at moderate and high E_b/N_0 values. At the same time, the proposed CIOD-MBM schemes offer a flexible design opportunity for varying N_t and N_{rf} values under $N_r = 4$. For $\eta = 4$ bit/s/Hz, although CIOD-MBM I has larger N_{rf} than CIOD-MBM II under the same N_t, N_r, and M, both schemes provide nearly the same error performance. For $\eta = 4.5$ and $\eta = 6.5$ bit/s/Hz, CIOD-MBM II provides a remarkable increase in BER performance compared to CIOD-MBM I since higher spectral efficiency values are easily obtained even with a small increase in N_t and N_{rf} values. The main difference between the two proposed schemes is CIOD MBM II scheme's ability to achieve a similar spectral efficiency and BER with a less number of antennas.

Fig. 3 depicts the BER of the proposed schemes against the BER of conventional CIOD, CIOD-SM and MBM for $\eta = 4$ bit/s/Hz. Here, degree of SM (DoSM) scheme, which is defined in [17], is considered as CIOD-SM. It should be noted that all reference schemes use a single RF chain during the transmission for a fair comparison. As can be clearly seen, CIOD-MBM I scheme provides around 5 dB supremacy over CIOD and approximately 10 dB over CIOD-SM, SIMO and MBM schemes. At the same time, CIOD-MBM II scheme provides similar error performance with CIOD-MBM scheme for $\eta = 4$ bit/s/Hz while providing better error performance for higher spectral efficiency values as in Fig. 2. It should be noted that the CIOD-MBM schemes do not impose any restriction on N_t and N_{rf} values. The increased spectral

$$\mathbf{H}_{eq} = \begin{bmatrix} h_{1,m_1}^{\Re} & h_{2,m_1}^{\Re} & \dots & h_{N_r,m_1}^{\Re} & h_{1,m_1}^{\Im} & \dots & h_{N_r,m_1}^{\Im} & 0 & \dots & 0 & 0 & \dots & 0 \\ 0 & 0 & \dots & 0 & 0 & \dots & 0 & h_{1,m_2}^{\Re} & \dots & h_{N_r,m_2}^{\Re} & h_{1,m_2}^{\Im} & \dots & h_{N_r,m_2}^{\Im} \\ 0 & 0 & \dots & 0 & 0 & \dots & 0 & -h_{1,m_2}^{\Im} & \dots & -h_{N_r,m_2}^{\Im} & h_{1,m_2}^{\Re} & \dots & h_{N_r,m_2}^{\Re} \\ -h_{1,m_1}^{\Im} & -h_{2,m_1}^{\Im} & \dots & -h_{N_r,m_1}^{\Im} & h_{1,m_1}^{\Re} & \dots & h_{N_r,m_1}^{\Re} & 0 & \dots & 0 & 0 & \dots & 0 \end{bmatrix}^T \quad (14)$$

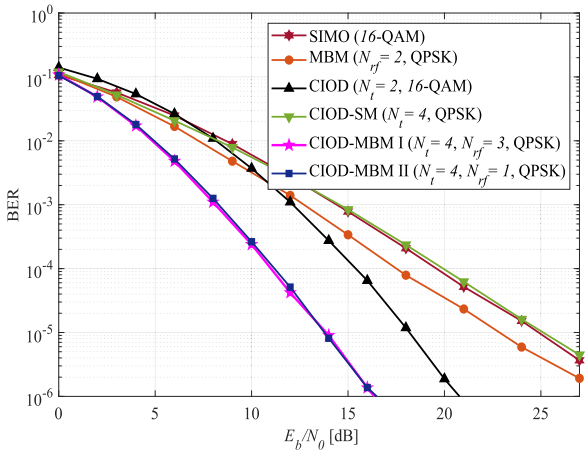

Fig. 3. The BER of the proposed CIOD-MBM schemes compared to the reference systems with $N_r = 2$ receive antennas for about $\eta = 4$ bit/s/Hz.

efficiency and data rates are obtained by easily increasing N_t and N_{rf} for both schemes while keeping the M constant. Moreover, to meet the high data rate demand in next-generation communication systems, increasing N_{rf} instead of N_t and M will reduce hardware costs. Moreover, reconfigurable antenna designs play a critical role in leverage from the benefits of the MBM method since imperfect antenna designs may lead to correlated channel conditions, leading to a degradation in error performance.

V. Conclusion

In this paper, CIOD-MBM concept has been introduced to increase the spectral efficiency of conventional CIOD and MBM schemes by using CIOD as an additional information source as well as transmit antennas, channel states, and amplitude/phase modulation. One of the most weighty benefits of the CIOD-MBM schemes, which promise high data rates by using a low number of transmit antennas, is enabling reduced receiver complexity by symbol-by-symbol detection. As a result of theoretical ABEP and computer simulations, it has been shown that proposed CIOD-MBM schemes provide superiority to reference systems in terms of error performance. Derivation of closed-form BER expression and investigation of antenna design limitations will be our future endeavors.

References

[1] T. Mao, Q. Wang, Z. Wang, and S. Chen, "Novel index modulation techniques: A survey," *IEEE Commun. Surv. Tut.*, vol. 21, no. 1, pp. 315–348, Jan.-Mar. 2018.

[2] J. Jeganathan, A. Ghrayeb, and L. Szczecinski, "Spatial modulation: Optimal detection and performance analysis," *IEEE Trans. Wireless Commun.*, vol. 12, no. 8, pp. 545–547, Aug. 2008.

[3] E. Seifi, M. Atamanesh, and A. K. Khandani, "Media-based MIMO: Outperforming known limits in wireless," in *Proc. IEEE Int. Conf. Commun.*, Kuala Lumpur, Malaysia, May 2016, pp. 1–7.

[4] Y. Naresh and A. Chockalingam, "On media-based modulation using RF mirrors," *IEEE Trans. Veh. Technol.*, vol. 66, no. 9, pp. 4967–4983, Jun. 2016.

[5] I. Yildirim, E. Basar, and I. Altunbas, "Quadrature channel modulation," *IEEE Wireless Commun. Lett.*, vol. 6, no. 6, pp. 790–793, Aug. 2017.

[6] E. Basar and I. Altunbas, "Space-time channel modulation," *IEEE Trans. Veh. Technol.*, vol. 66, no. 8, pp. 7609–7614, Aug. 2017.

[7] B. Shamasundar, S. Bhat, S. Jacob, and A. Chockalingam, "Multidimensional index modulation in wireless communications," *IEEE Access*, vol. 6, pp. 589–604, Nov. 2017.

[8] I. Yildirim, E. Basar, and G. K. Kurt, "Media-based modulation for secrecy communications," *Electron. Lett.*, vol. 54, no. 12, pp. 789–791, Jun. 2018.

[9] Y. Naresh and A. Chockalingam, "A low-complexity maximum-likelihood detector for differential media-based modulation," *IEEE Commun. Lett.*, vol. 21, no. 10, pp. 2158–2161, Oct. 2017.

[10] S. Lu, I. A. Hemadeh, M. El-Hajjar, and L. Hanzo, "Compressed-sensing-aided space-time frequency index modulation," *IEEE Trans. Veh. Technol.*, vol. 67, no. 7, pp. 6259–6271, 2018.

[11] S. Jacob and A. Chockalingam, "Detection of generalized media-based modulation signals using multi-layered message passing," in *Proc. IEEE 87th Veh. Technol. Conf.*, 2018, pp. 1–5.

[12] Z. Yigit and E. Basar, "Space-time media-based modulation," *IEEE Trans. Signal Process.*, vol. 67, no. 9, pp. 2389–2398, May 2019.

[13] I. Yildirim, E. Basar, and I. Altunbas, "Fractional media-based modulation with golden angle modulation," in *Proc. IEEE Wireless Commun. Netw. Conf. Workshop*, Apr. 2019, pp. 1–5.

[14] Z. A. Khan and B. S. Rajan, "Space-time block codes from co-ordinate interleaved orthogonal designs," in *Proc. IEEE Int. Symp. Inf. Theory*, Lausanne, Switzerland, 2002, p. 275. [Online]. Available: https://ieeexplore.ieee.org/document/1023547

[15] M. Simon and M. S. Alaouni, *Digital Communications Over Fading Channels*. New York: NY, USA, Wiley, 2005.

[16] G. L. Turin, "The characteristic function of hermitian quadratic forms in complex normal variables," *Biometrika*, vol. 47, no. 1/2, pp. 199–201, Jun. 1960.

[17] R. Rajasker and K. V. S. Hari, "Modulation diversity for spatial modulation using complex interleaved orthogonal design," in *Proc. IEEE TENCON*, Cebu, Philippines, Nov. 2012, pp. 1–6.